1

Seasonal Mixed-Layer Temperature in the Congolese Upwelling System (CUS)

R.D. Ngakala[1,2], G. Alory[3], C.Y. Da-Allada[1,4,5], I. Dadou[3], C. Cardot[3], G. Morvan[3], J. Jouanno[3], S. Illig[3,6], and E. Baloïtcha[1]

[1]Department of Oceanography and Applications, International Chair in Mathematical Physics and Applications, University of Abomey-Calavi, Cotonou, Benin.

[2]Department of Oceanography and Environment, Institut National de Recherche en Sciences Exactes et Naturelles, Pointe-Noire, Congo.

[3]Université de Toulouse, LEGOS (CNES/CNRS/IRD/UPS), Toulouse, France.

[4]Laboratoire de Géosciences, de l'Environnement et Applications, Université Nationale des Sciences Technologies, Ingénierie et Mathématiques, Abomey, Benin.

[5] Laboratoire d'Hydrologie Marine et Côtière, Institut de Recherches Halieutiques et Océanologiques du Bénin, Cotonou, Benin.

[6] Department of Oceanography, University of Cape Town, Cape Town, Rondebosch, South Africa.

Corresponding author: R.D. Ngakala (roy.ngakala@gmail.com)

Key Points:

- Competition between solar flux inducing heating and vertical mixing at the base of the mixed-layer inducing cooling in the Congolese upwelling system (CUS).
- Seasonal cooling induced by vertical mixing, not controlled by the local wind, but rather by remotely forced coastal trapped waves via the rise of the thermocline and the strengthening of the vertical temperature gradient at the base of the mixed-layer in the CUS.

Abstract

The Congolese upwelling system (CUS), located along the West African coast north of the Congo River, is one of the most productive and least studied systems in the Gulf of Guinea. The Sea Surface Temperature minimum in the CUS occurs in austral winter, when the winds are weak and not particularly favorable to coastal upwelling. Here, for the first time, we use a high-resolution regional ocean model to identify the key atmospheric and oceanic processes that control the seasonal evolution of the mixed-layer temperature in a 1°-wide coastal band from 6°S to 4°S. The model is in good agreement with observations on seasonal timescales, and in particular reproduces the signature of the surface upwelling during the austral winter, the shallow mixed-layer due to salinity stratification, and the signature of coastal wave propagation. The analysis of the mixed-layer heat budget reveals a competition between warming by air-sea fluxes, dominated by the solar flux throughout the year, and cooling by vertical mixing at the base of the mixed-layer, as other tendency terms remain weak. The seasonal cooling is induced by vertical mixing, but is not controlled by the local wind. A subsurface analysis shows that remotely-forced coastal trapped waves raise the thermocline from April to August, which strengthens the vertical temperature gradient at the base of the mixed-layer and leads to the mixing-induced seasonal cooling in the Congolese upwelling system.

Plain Language Summary

The Congolese upwelling system is located along the West African coast north of the Congo River. It is one of the highly productive systems in the Gulf of Guinea and has received the least attention due to the lack of historical data in this coastal region. The low temperatures occur during the austral winter when winds are weak in the area. We use a high-resolution regional ocean model to identify the main atmospheric and oceanic forcing controlling the seasonal changes in sea surface temperature. We find a competition between warming by air-sea fluxes, dominated by the solar flux throughout the year, and cooling by vertical mixing. The seasonal occurrence of low temperature induced by vertical mixing is not controlled by the local wind, but rather by remotely forced coastal trapped waves.

Acronyms:

CTW: Coastal trapped waves

CUS: Congolese Upwelling System

EKW: Equatorial Kelvin Waves

GG: Gulf of Guinea

ILD: Isothermal Layer Depth

MLD: Mixed Layer Depth

MLT: Mixed Layer Temperature

SSS: Sea Surface Salinity

SST: Sea Surface Temperature

TD: Thermocline Depth

1 Introduction

The Congolese upwelling system (CUS), located along the western African coast between 6°S and 4°S, just north of the mouth of the Congo River, is one of the most productive systems in the Gulf of Guinea (GG), and likely has a strong influence on regional fisheries (Voituriez & Herbland, 1982). The low Sea Surface Temperature (SST) in the CUS occurs in austral winter (June-July-August), when the winds favorable to Ekman upwelling are weak (Berrit, 1976) as in the Angola upwelling system (Ostrowski et al., 2009; Awo et al., 2022), which suggests that it is not associated with wind-driven Ekman transport, unlike the Benguela upwelling system further south (Carr and Kearns, 2003; Gutknecht et al., 2013; Bordbar et al., 2021). The equatorial undercurrent (EUC), which extends into the Gabon-Congo Coastal Undercurrent (GCUC) flowing southeastward, probably brings the source waters for the CUS (Wacongne & Piton, 1992). At the eastern boundary of the Atlantic, the termination of the equatorial current systems between the EUC through the GCUC at the subsurface and the South Equatorial Current (SEC) at the surface could induce an upwelling of coastal waters (Piton, 1988), thus affecting the SST. In the CUS, seasonal changes in SST can also be affected by eastward propagating equatorial Kelvin waves (EKW) triggering southward propagating coastal trapped waves (CTW), as shown recently in the Cape Lopez region (Herbert and Bourlès, 2018) north of the CUS. The influence of CTWs has already been highlighted in the Angola and Benguela upwelling systems (Bachèlery et al., 2016; Illig et al., 2020; Körner et al., 2023) located further south of the Congo River mouth. Analysis of altimetry and tide gauges data as well as model outputs reveals also the semi-annual cycle for sea level anomalies associated with CTW along the coast of Africa in the Gulf of Guinea (Dieng et al., 2021). The CUS is also probably under the influence of the Congo River plume, a large tongue of low-salinity water as well as sediment, organic matter and nutrient charged. Indeed, the plume, driven by the topography, the Coriolis effect, and prevailing winds, generally extends northwestward, partially covering the Congolese continental shelf and is potentially associated with mesoscale activity (Denamiel et al., 2013; Vic et al., 2014). Because of the shallow mixed-layer (MLD) due to the strong salinity stratification near the surface, the plume can inhibit vertical mixing, which can reduce upwelling and nutrient flux to the surface (Voituriez and Herbland, 1982; Dossa et al., 2019; Houndegnonto et al., 2021; Topé et al., 2023). Materia et al., (2012) associated positive interannual SST anomalies with years of high Congo River discharge and high precipitation in the GG from observational analysis. Contrary to Materia et al. (2012), White and Toumi (2014) show that the Congo River impacts on SST are limited in coastal regions under the influence of the River plume, and their modeling results are in agreement with the previous analysis of Hopkins et al. (2013) based on satellite observations. The impact of high stratification due to River plume has been highlighted to explain the warm event in 2016 off the coast of Angola (Lübbecke et al., 2019), in agreement with the interannual Congo river plume southward extension deduced from satellite Sea Surface Salinity (SSS) (Martins and Stammer, 2022). On the contrary, the density front around the Congo estuary could locally create upwelling through the secondary ageostrophic circulation (Pham & Sarkar, 2018). The Congo plume could also induce coastal geostrophic divergence to its north, mirroring the effect of the Niger River the other side of the equator, with possible upwelling enhancement (Alory et al., 2021). The seasonal SST minimum coincides with a maximum in chlorophyll-a (CHL-a) concentrations north of the Congo, like in other coastal regions of the GG (Brandt et al., 2023). Thus, understanding the

seasonal variability of SST will also provide some insight on certain processes involved in nutrient flux and thus productivity in the CUS.

Contrary to the Angola and Benguela systems that have received more attention, the dynamics of the mixed-layer temperature (MLT) in the CUS is still debated. Several studies have focused on the impact of the Congo River at the scale of the tropical Atlantic basin. For example, Da-Allada et al. (2014) and Camara et al. (2015) used an ocean model to analyze seasonal changes in mixed-layer salinity in large regions of the tropical Atlantic. In the southern GG including the Congo River plume area, their results reveal that diffusion and vertical advection act against the action of horizontal advection and freshwater fluxes (mainly dominated by the Congo River) that freshen the mixed-layer. These results are also in agreement with those of Houndegnonto et al. (2021) based on SMOS (Soil Moisture and Ocean Salinity) satellite observations. Also, the studies carried out to understand the seasonal cycle of the MLT have been limited to the larger regions around the Congo River. Using PIRATA (Prediction and Research Moored Array in the Tropical Atlantic, Bourlès et al., 2019) mooring data, Foltz et al. (2003) showed that the seasonal cycle of the MLT is controlled by the net surface heat flux, mainly the solar flux and the latent heat flux along 10°W at 10°S and 6°S. Peter et al. (2006) also found in numerical simulations that the mixed-layer heat budget is governed by the net surface heat flux in the southern GG, and particularly at 3°E, between 8°S and 4°S. The dominant role of net surface heat flux is also confirmed by Wade et al. (2011) in their box extending from 3°E to the African coast, between 10°S and 4°S. In addition, from simulated mixed-layer heat budget, Ngakala et al. (2023) have also underlined this dominant role of net surface heat flux along the African coast, especially in the Senegal, Angola and Benguela regions. Also, Scannell and McPhaden (2018) used data from a PIRATA mooring located off the Congo River at [8°E; 6°S] to understand seasonal changes in MLT. Their results show that the seasonal variations of the net surface heat flux are strongly governed by the solar flux and the latent heat flux whose variations are influenced by the meridional displacement of the intertropical convergence zone (ITCZ) and the formation of marine stratocumulus at low altitude. In boreal spring, they associate the warming of the mixed-layer with the action of the solar flux amplified by the shallow MLD due to heavy precipitation and the freshwater input from the Congo River. In austral winter, they attribute the cooling of the MLD to turbulent vertical entrainment (although not explicitly resolved) favored by upwelling conditions. Their study suggests the importance of taking into account precipitation to understand the mixed-layer heat budget in the southeast Atlantic ocean because of their effect on the MLD. Also, results from experiments based on simulations (with and without the Congo River) by White and Toumi (2014) suggested that the Congo River induces all year long a slight cooling in the plume by shallowing of the MLD, which reduces the short wave absorption within the mixed layer.

Further south, using available observations, Körner et al. (2023) conducted a heat budget to understand the processes responsible for the cross-shore SST gradient observed in the Angolan upwelling system. Their results have shown that cooling by turbulent mixing at the base of the mixed-layer is stronger at the coast in the shallow regions of the shelf than offshore. However, the net surface heat flux attenuates the spatial differences in SST by inducing a stronger warming at the coast.

Here, we use for the first time a high-resolution regional ocean model to determine the main atmospheric and oceanic processes that control the seasonal evolution of the MLT in the CUS. We focus our study along the Congolese coast between 6°S and 4°S, in the 1°-wide coastal

band to capture the influence of coastal trapped waves (Illig, 2004; Bachèlery et al., 2016). In addition, we will evaluate if the seasonal cooling is associated with local forcing and/or remote oceanic forcing (coastal trapped waves). In the following, we describe the observations, the model and the methodology used in section 2. Then, we will present the results concerning the model's ability to reproduce the observations, the analysis of the MLT seasonal cycle and various processes involved in section 3. Finally, sections 4 and 5 are devoted to the discussion and conclusion respectively.

2 Data, Model and Methods

2.1 Data

Satellite and *in situ* observations are used to evaluate the ability of the model to realistically simulate the spatial and seasonal variations of some key surface and subsurface fields, such as SST, SSS, sea level anomalies (SLA), temperature.

- The Multi-scale Ultra-high Resolution (MUR) satellite product with 1/100° spatial resolution (~ 1 km) and daily temporal resolution (Chin et al., 2017) is used to assess the realism of the model SST. This product is an optimal combination of SST data from infrared and microwave sensors.

- The observed SSS is derived from the Soil Moisture Active Passive (SMAP) satellite product with 1/4° (~25 km) spatial and daily temporal resolution, which is obtained from a temporal extrapolation of 8-day products (Fore et al., 2016).

Although both of these satellite products have a daily resolution, we used the monthly MUR and SMAP products to validate the model SST over the period 2007-2016 (10 years) and SSS over the period 2016-2022 (i.e. 7 years, due to the availability of the SMAP product), respectively.

- The CMEMS (Copernicus Marine Environment Monitoring Service) altimetry product, which combines data from several satellite missions with 1/4° spatial and daily temporal resolution (Le Traon et al., 1998; Ducet et al., 2000), helped to evaluate the model SLA. For a better comparison between the model and the CMEMS product, we computed the SLA from the daily sea surface height over a common reference period (2007-2016). This SLA product is then used to assess the ability of the model to track the EKW eastward propagations and the subsequent CTW southward propagation along the African coast.

- SSS from underway thermosalinographs (TSG) collected during 6 crossings of the Hawk Hunter commercial ship and 3 PIRATA cruises onboard French research ship in the Gulf of Guinea on the June-July-August season between 2000 and 2021 are averaged along transects repeated at last 3 times (Alory et al., 2015; Gaillard et al., 2015; Bourlès et al., 2019).

- In situ monthly climatological data from World Ocean Atlas 2018 (WOA18) with a horizontal resolution of 1/4° (~ 25 km) and a vertical resolution of 5 m in the first 100 m (Garcia et al., 2019) are used for subsurface temperature validation.

- In addition, we used daily in situ data from the PIRATA mooring (Rouault et al., 2009) located off the mouth of the Congo River at [8°E; 6°S] over the 3-year period of 2014-2016 to consolidate the model validation in surface and subsurface. Following Scannell and McPhaden

(2018), we first applied orthogonal linear least squares regression between 10 and 1 m and then 10 and 1 m to fill in the data gap for salinity at 1 and 5 m depth in 2016. And second, we linearly interpolated along the vertical with 1 m resolution from temperature and salinity profiles at depths of 1, 5, 10, 20, 40, 60, 80, 100, and 120 m. From this new time series, the associated subsurface daily density is computed and then the mixed-layer depth and isothermal layer depth (ILD) are determined following Scannel (2018) using a density criterion (0.08 kg/m^3) and temperature criterion (0.3 °C), respectively, relative to a reference depth of 1 m.

2.2 Model

We use a regional configuration of the NEMO ocean model (Nucleus for European Modeling of the Ocean, Madec et al., 2017) to understand the thermodynamics in the Congolese upwelling system. The regional simulation covers the Gulf of Guinea from 11°S to 6°N, and from 10°W to the west African coast. The model solves the discretized primitive equations on a horizontal Arakawa C-grid following the GLS turbulent closure scheme, with a horizontal resolution of 1/36° (~ 3 km). The vertical grid, in z coordinates, has 50 levels with 18 levels in upper 50 m. The model is forced by daily MERCATOR GLORYS12V1 reanalysis outputs (Jean-Michel et al., 2021) with a horizontal resolution of 1/12° (~ 9 km) at its lateral open boundaries. Atmospheric fluxes used for surface forcing are from the Japanese Meteorological Agency JRA-55 reanalyzes (Kobayashi et al., 2015), except for the daily surface winds which are from the ASCAT satellite product with a horizontal resolution of 1/4° or ~ 25 km (Bentamy and Fillon, 2012). The river runoff forcing for the model is provided by the daily outputs of the ISBA-CTRIP hydrological model (Decharme et al., 2019), except at the mouth of the Congo River (around 6°S), where the runoff is based on the daily flows measured by the Brazzaville station managed by the HYBAM network (HYdro-geochemistry of the AMazonian Basin) (Laraque et al., 2020). The simulation was run from 2005 to 2016 including two years of spin-up (2005-2006, initialized with GLORYS in 2005). The heat budget terms are computed online (5-min time step) at each depth level for year 2016. The processes driving the seasonal changes of MLT along the Congolese coasts are inferred from the analysis of year 2016 year, due to the availability of heat budget terms. The interannual variability mode of SST over the 2007-2016 period shows that 2007 and 2016 years are relatively warm compared to other years (not shown) in our study region. This warm event in early 2016 was investigated in a previous study based on observations (in situ and satellite) in the southeastern tropical Atlantic off the coast of Angola and Namibia (Lübbecke et al., 2019). In the following, we will take into account this particularity of year 2016. Note that this model configuration, with slightly different forcing, has already been used to study the impact of the Niger River warming effect in coastal upwelling systems north of the GG (Topé et al., 2023).

2.3 Methods

The processes locally controlling the mixed-layer temperature along the Congolese coast within a 1°-wide band from the coast are examined from the mixed-layer heat budget. This approach has already been used in several studies based either on observations (Wade et al., 2011; Scannell & McPhaden, 2018) or with our model (Peter et al., 2006; Jouanno et al., 2011). The evolution of the MLT is given by **Eq.1**:

$$\partial_t\langle T\rangle = \underbrace{\frac{Q^*+Q_s(1-f_{z=-h})}{\rho_0 c_p h}}_{A} \underbrace{-\langle u.\partial_x T\rangle - \langle v.\partial_y T\rangle + \langle D_l(T)\rangle}_{B} \underbrace{-\langle w.\partial_z T\rangle - \frac{(k_z\partial_z T)_{z=-h}}{h} - \frac{1}{h}\partial_t h(\langle T\rangle - T_{z=-h})}_{C} \quad (1)$$

where T is the potential temperature, (u, v, w) are the zonal, meridional, and vertical components of the velocity vector, and k_z the vertical diffusion coefficient parametrized in the model following the Generic Length Scale (GLS) scheme (Umlauf and Burchard, 2003, 2005). $< >$ denotes the averaged quantities in the mixed-layer of depth h. We calculated the MLD from daily outputs following a density criterion with 0.5 m (first level of the model) as reference level and 0.08 kg/m³ as threshold from daily vertical profile outputs as done in Scannell and McPhaden (2018), and integrated vertically the online heat budget terms over this MLD. In the discussion section, we will return to the choice and the sensitivity of the MLD criterion.

The left side of equation (1) represents the mixed-layer temperature tendency term, and the right side represents all terms contributing to the mixed-layer heat budget. A is the net surface forcing due to non-solar surface fluxes (sum of longwave, latent and sensible heat fluxes, $\boldsymbol{Q}^*$) and the penetrating solar flux ($\boldsymbol{Q_s}$). B is the horizontal oceanic processes: the horizontal advection, composed of zonal and meridional components, and the lateral diffusion. C represents the sum of the vertical oceanic processes: *i.e.* vertical advection, vertical diffusion at the base of the mixed-layer, and entrainment. The latter represents temperature variations within the mixed-layer due to changes in mixed-layer thickness and is estimated as a residual to close the mixed-layer budget (Jouanno et al., 2011).

In addition, we also investigated the link between surface and subsurface dynamics at the seasonal scale based on the three-dimensional (x-zonal, y-meridional, z-vertical) online heat budget detailed in **Eq.2**. This showed how the MLT seasonal changes are related to the subsurface dynamics and also underlined the sensitivity of the mixed-layer heat budget terms to the choice of the reference depth.

$$\partial_t T = \underbrace{\frac{Q^*+Q_s\times f(z)}{\rho_0 c_p}}_{A} \underbrace{-u.\partial_x T - v.\partial_y T + D_l(T)}_{B} \underbrace{-w.\partial_z T - \partial_z(k_z\partial_z T) + Res(z)}_{C} \quad (2)$$

In **Eq.2**, the terms A, B, and C are similar to those described in **Eq.1**, but at each model vertical level, not averaged in the mixed layer. A has a vertical and decaying structure and depends on non-solar fluxes only at the surface. The term C, denoted Res(z), is the residual and include the numerical diffusion term due to the temporal scheme. Res(z) is very small and will be disregarded.

Since seasonal changes in the MLT can also be influenced by remote forcing, such as the equatorially-forced CTW, we analyze its signature along the equatorial band (8°W – 12°E, 1°S – 1°N) and along the Congolese coast (1°-wide coastal band between 6°S - 4°S) using SLA from both observations and the model, and also examine thermocline depth (TD) variations in the model. Previous studies have often used the 20°C isotherm as a proxy for the thermocline depth noted by Z_{20} (Lübbecke et al., 2019; Herbert and Bourlès, 2018). Here, we used the depth corresponding to the daily maximum vertical temperature gradient at each grid point below the isothermal layer as a proxy for TD. We found this criteria to be a better proxy than Z_{20} for the thermocline depth in our coastal area influenced by the vertical salinity gradient (not shown).

3 Results

3.1 Evaluation of model skills

3.1.1 Surface evaluation from satellite data

In austral winter (June-July-August), the model (**Figure 1b**) qualitatively reproduces the average SST conditions observed by the MUR satellite product (**Figure 1a**) in our study region. Indeed, the spatial analysis shows warm SSTs offshore and cold SSTs at the coast, so we find the characteristics of regions dominated by upwelling systems like EBUS (Chavez and Messié, 2009) in both observations and model. This cooling could also be associated with the contribution of CTW as mentioned in the studies of Angola and Benguela upwelling systems (Bachèlery et al., 2016, 2020). This cooling has a wider cross-shore extension and a more homogeneous alongshore extension in the observations than in the model. In the model, it is clearly accentuated on each side of the Congo River mouth, which is slightly visible in the MUR product. Although the model and observations show similar large-scale structures, the model remains warmer offshore with a positive bias of about 1°C relative to the MUR product. These differences can be attributed to either the MUR product or the model. For example, the heat fluxes used or lateral forcing at western boundary to force the model or again insufficient sub-surface cooling can overestimate the SST and be the source of this larger difference offshore relative to the coast. Note that a warm bias in SST is often mentioned in the southeastern tropical Atlantic, and this bias is likely either atmospheric in origin, such as excessive shortwave radiation due to poor cloud representation, or oceanic in origin, such as the misrepresentation of ocean dynamics (Xu et al., 2014; Richter, 2015; Deppenmeier et al., 2020; Kurian et al., 2021).

The model successfully reproduces the main features of the SSS (**Figure 1d**) on a large scale as observed by SMAP satellite product (**Figure 1c**). We find saltier waters offshore and fresher waters at the coast due to the freshwater input from the Congo River. The model also captures well the northwestward extension of the Congo River plume (bounded by the 32 psu isohaline) associated with the southeast trade winds regime in agreement with previous studies in the region (Denamiel et al., 2013; Vic et al., 2014). Despite the model representing similar patterns of the observed mean SSS, it remains fresher than the SMAP mean and this negative bias is amplified at the coast. These differences can be partially explained by the freshwater fluxes (dominated here by the Congo runoff) used as model forcing. The model also simulates freshwater in the plume and saltwater out of the plume, as measured along TSG transects from commercial ships and PIRATA cruises. Differences could be due to inter-annual variability and low sampling density (often a few hours or days).

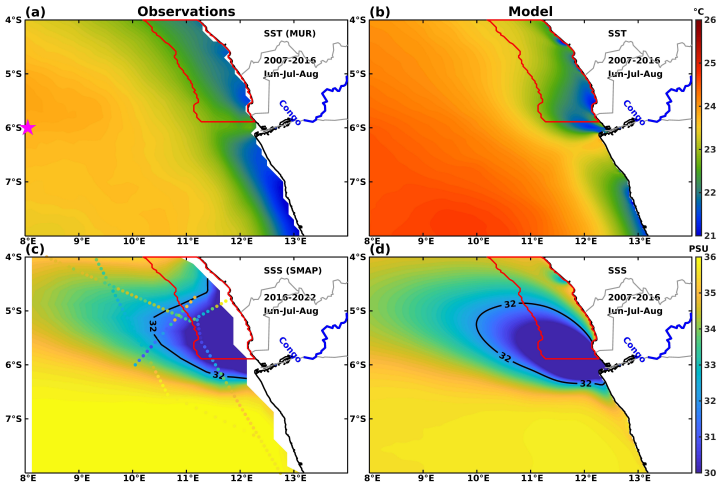

Figure 1. Mean austral winter (Jun-Jul-Aug) surface conditions (Sea Surface Temperature (°C, top panels) and Sea Surface Salinity (PSU, bottom panels)) over the period 2007-2016 (except for SMAP SSS: 2016-2022) for observations (a for MUR SST and c for SMAP SSS) and model SST (b) and SSS (d). Colored tracks in panel c are SSS from repeated TSG and 3 PIRATA cruise transects during the period 2000-2021. The 32 PSU isohaline delineates the extent of the Congo river plume. The red contour represents the 6°S-4°S 1°-wide coastal box used in **Fig.4**, **Fig.8**, and **Fig.9**. The blue line is the Congo River and the magenta star in panel a is the PIRATA mooring position at [8°E; 6°S].

Analysis of the coastal (1°-wide coastal band) monthly climatology of SST and SSS highlights the surface signature of the upwelling during the austral winter in both satellite products (**Figure 2a-b**) and model (**Figure 2c-d**). In **Figure 2a-d**, cold SSTs (<22°C) are observed between June and August, and warm SSTs during the rest of the year. SSTs increase from September to a maximum (~28°C) between February and March, and decrease from April. North of 5°S (**Figure 2b-d**), the SSS structure appears to be influenced by the combined coastal rainfall and Congo River regime. Saltier water is observed from May to early September, and fresher water appears during the rest of the year corresponding to the periods of maximum Congo River discharge (October-November-December) and coastal rainfall (February-March), consistent with previous studies in the Congo River area (Houndegnonto et al., 2021; Awo et al., 2022). South of the Congo River from 6.5°S (less influenced by the Congo River than the north), fresher waters is observed from December to March and saltier waters during the rest of the year. The freshest waters due to the Congo River, presumably associated with strong salinity stratification, are found between 5°S-6.5°S throughout the year. And this signature due to the Congo River is strongly pronounced in the model compared to the SMAP product.

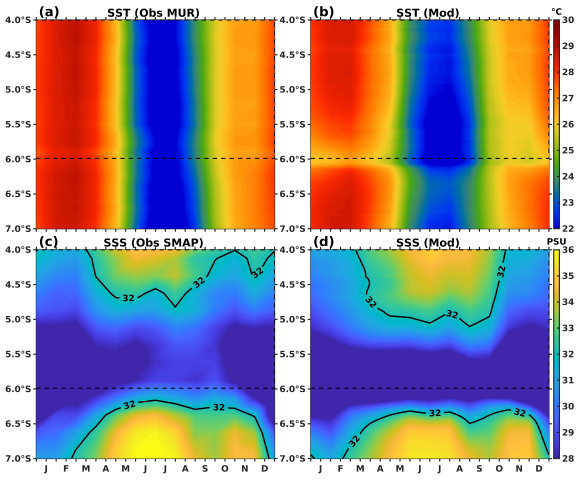

Figure 2. Monthly climatology of coastal (averaged within the 1°-wide coastal band) surface conditions (SST (°C, top panels) and SSS (PSU, bottom panels)) estimated over the period 2007-2016 (except for SMAP SSS: 2016-2022) for observations (a for MUR SST and c for SMAP SSS) and model SST (b) and SSS (d). The dashed line at 6°S highlights the location of the mouth of the Congo River.

Above, we have shown that the coldest SSTs occur in June-August when winds favorable for Ekman upwelling are relatively weak (not shown here), which is consistent with studies along the African coast in the southern tropical Atlantic (Berrit, 1976; Ostrowski et al., 2009; Herbert and Bourlès, 2018; Lübbecke et al., 2019), suggesting that CTW could play a role on the SST seasonal variability. Therefore, we examine the seasonal signature of long waves on the SLA and thermocline depth (TD) respectively along the equator (EKW eastward propagation) and along the African coast in the south (CTW southward propagation) in observations and model. The wave signature on the SLA is clearly visible in the CMEMS satellite product (**Figure 3a-b**) and the model (**Figure 3d-e**). This signature can also be seen on the TD in the model (**Figure 3c-3f**). In the observations, negative SLA anomalies occur from May to August along the equator (**Figure 3a**) and along the southern coast (**Figure 3b**). Except for January between 7°W-1°W and December between 5°S-4°S, positive SLA anomalies are observed for the rest of the year. On the other hand, the negative SLA anomalies appear earlier in the model, from March to August along the equator and then from April to August along the coast. The model also reproduces the negative anomalies in early December, extending to about 5.5°S. There is a slight seasonal shift in the modeled negative SLA anomalies compared to the observed ones. At the equator, the model shows shallow TDs between April and August, the main period of negative SLA anomalies. Deeper TDs are found throughout the rest of the year, except east of 8°E. Along the coast, the model shows that shallow TDs occur around March and August, while deeper TDs occur throughout the year except from November to December south of 3°S.

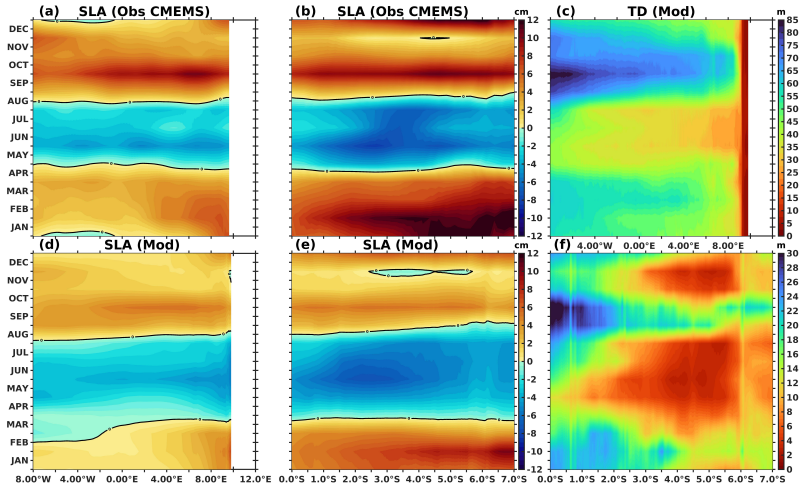

Figure 3. Eastern equatorial (averaged within 1°S-1°N, panels a, c, and d) and coastal (averaged within the 1°-wide coastal band, panels b, e, and f) monthly climatology of altimetry (CMEMS satellite product, panels a and b) and model (panels d and e) Sea Level Anomaly (SLA, cm). Panels c and f show the model monthly climatology of eastern equatorial and coastal Thermocline Depth (TD, m), respectively.

3.1.2 Sub-surface evaluation from in situ data

The upwelling signature is also visible in the subsurface in the *in situ* observations (**Figure 4a**) and in the model (**Figure 4b**) during austral winter by analyzing of the monthly climatology of the temperature averaged in our study box (1°-wide coastal fringe from 6°S to 4°S, see red contour in **Figure 1**). The model clearly reproduces the monthly evolution of the subsurface temperature observed in WOA climatology, and in particular the seasonal vertical displacements of the thermocline depth. The seasonal cycle of the observed and modelled vertical movements of the MLD, ILD, and TD are in phase. The observed and modeled MLD remain shallow (less than 3 m) all year. The ILD and TLD are maximum in October in both observations and model, but a secondary maximum in January is more pronounced in the WOA climatology than in the model and it occurs one month later in the model. The modeled thermocline rises from March and is shallower (~3 m) than observed (5 m) between June and August when SST is below 22°C. However, the model is slightly colder than the WOA climatology for most of the year. In the GG, several studies have mentioned that the haline stratification due to strong freshwater inputs from precipitation and river discharge can create barrier layers, that limit vertical exchanges between the surface and subsurface (Materia et al., 2012; Dossa et al., 2019; Houndegnonto et al., 2021). In our box, the ILD is deeper than the MLD leading to a barrier layer; the associated barrier layer thickness (BLT: difference between ILD and MLD) is negligible during the upwelling season but reaches about 3 m in February-March and 7 m in October, which is about twice the mixed-layer thickness. These differences may be related to the poor density sampling of in situ data in the Congo River region or model bias.

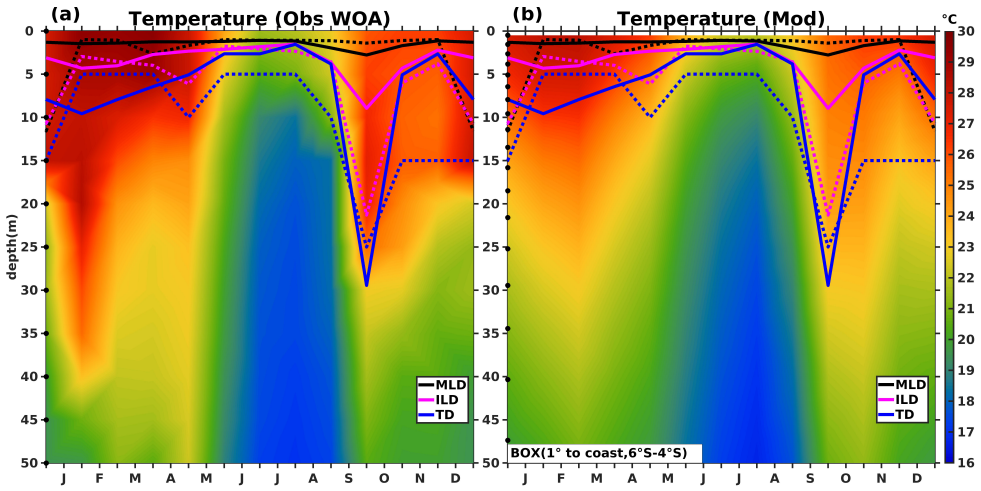

Figure 4. Subsurface (0-50m) temperature (°C) monthly climatology averaged within the 6°S-4°S 1°-wide coastal box (red contour in **Fig.1**) from a) WOA and b) the 2007-2016 model climatology. Black, magenta, and blue lines represent the MLD, ILD, and TD respectively for the observations (dashed lines) and the model (solid lines). Here, TD is obtained from spatially averaged monthly profiles, while MLD and ILD are obtained from monthly profiles.

Furthermore, the model also reproduces the seasonal evolution of the vertical profiles of temperature, salinity, and density observed by the PIRATA mooring at [8°E; 6°S] (**Figure 5**). In June-August, the mixed-layer cools (**Figure 5a-d**) and becomes saltier (**Figure 5b-e**), leading to denser waters (**Figure 5c-f**) during this period. This also corresponds to the third annual rise of the thermocline, from July until October, which then deepens steeply in both the PIRATA observations and the model. During the rest of the year, the mixed-layer becomes warmer and fresher, and thus less dense. Also, the MLD, ILD, and TD in the model show a seasonal cycle in agreement with the PIRATA observations, although all 3 layers are deeper in PIRATA, especially outside of the upwelling season. Consequently, the modeled and observed BLTs are in phase during the cycle and reach their maximum in November-December, which is larger in the model. Although the model reproduces the salinity increase with depth, it remains saltier than PIRATA from December to February around 25-30 m depth. Note that, due to the availability of the model outputs, MLD, ILD, and TD are calculated offline from monthly profiles, rather than from daily profiles as in PIRATA. This can partly explain the difference between model and observations.

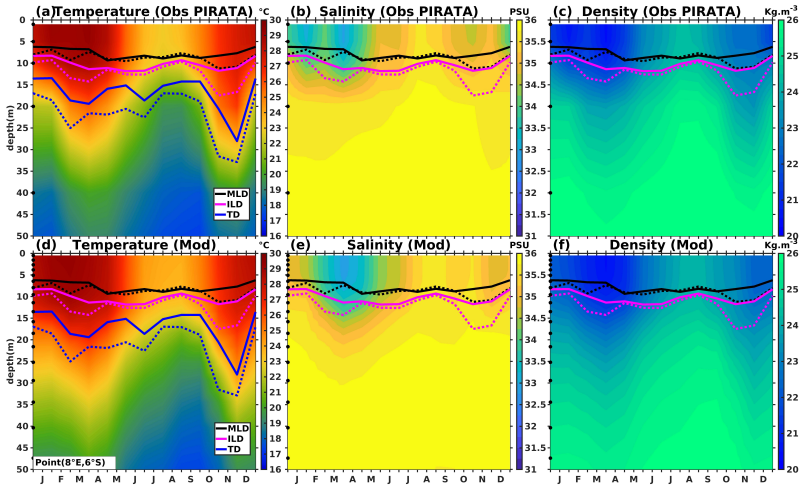

Figure 5. Subsurface (0-50m) monthly climatology of temperature (left panels, °C), salinity (middle panels, PSU), and density (right panels, kg.m^{-3}) at [8°E; 6°S] from PIRATA (top panels) and the model (bottom panels) for the period 2014-2016. Black, magenta, and blue lines represent the MLD, ILD, and TD, respectively, for the observations (dashed lines) and the model (solid lines). Due to the availability of the model outputs, the model MLD, ILD, and TD are computed offline from monthly profiles, rather than from daily profiles as for the PIRATA data.

Despite the differences between the model and the observations, the model reproduces the observed surface and subsurface upwelling signature quite well. Thus, we can rely on our model to evaluate the processes responsible for the seasonal change of the MLT along the Congolese coast and to analyze how the surface dynamics are related to the subsurface dynamics in the Congolese upwelling system.

3.2 Mixed-layer heat budget analysis

3.2.1 Processes driving the mixed-layer temperature seasonal changes

In this section, we analyze the processes involved in the seasonal variation of the mixed-layer temperature (**Figures 6 and 7**) with a focus on the ocean fringe along the Congolese coast. We use the model heat budget averaged within the mixed-layer (see **section 2.3**) to quantify the dominant processes responsible for the observed cooling in the Congolese upwelling system (CUS). Note that lateral diffusion and entrainment contributions are found to be very weak compared to other process contributions (not shown).

As expected, the climatology of the coastal MLT (**Figure 6a**) is very similar to the SST cycle (**Figure 2a-c**) along the coast. North of 6°S, we observe cold waters below 23.5 °C between June and September, and warm waters the rest of the year. The mixed-layer temperature tendency **Figure 6b** shows mainly a cooling (negative values) between March and July and a warming (positive values) the rest of the year. However, we note a warming between 7°S-6°S and then close to 5.5°S in April, another warming around 4.75°S-4°S in May, and a cooling around 6.15°S-5.5°S in December. These seasonal changes in the tendency term reflect the balance of processes that drive the variations in the MLT. Air-sea heat fluxes (**Figure 6c**) warm the mixed-layer throughout the year, and this means that the solar fluxes are dominant compared

to non-solar fluxes (latent heat, longwave, and sensible heat), which have a cooling effect. At the coast, the surface forcing (term A in **Eq.2**) variations are also controlled by the MLD associated with the strong salinity stratification of the Congo River discharge. A shallow MLD tends to trap the incoming solar flux in the first few meters at the surface, which probably explains the maximum in the river plume area just north of 6°S. As a result, the seasonal cooling is clearly due to oceanic processes (**Figure 6d**), which cool the MLD throughout the year and exceed the warming of the air-sea heat flux in March-July. The contribution of the horizontal processes (term B in **Eq.2**, **Figure 7a**) remains weak compared to that of the vertical processes (term C in **Eq.2**, **Figure 7d**). North of 6°S, zonal advection (**Figure 7b**) cools throughout the seasonal cycle, and its effect is reduced or slightly enhanced by meridional advection (**Figure 6c**), which either warms or cools depending on the latitude during the season. Vertical advection (**Figure 7e**) mostly cools the mixed-layer but its contribution is very weak compared to the vertical diffusion contribution (**Figure 7f**). The latter mainly controls the seasonal cycle of vertical processes, so it is vertical diffusion that is responsible for the coastal cooling of the MLT between March and July.

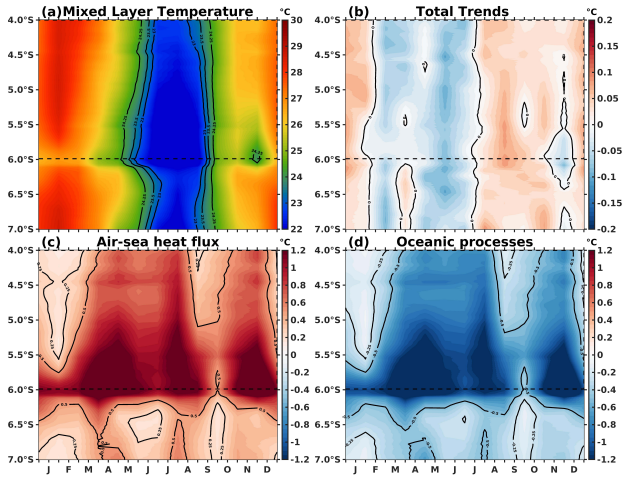

Figure 6. Model seasonal coastal mixed-layer heat budget for the year 2016: a) mixed-layer temperature (MLT, in °C), b) mixed-layer temperature tendency (in °C.day^{-1}), c) net surface forcing term (A in **Eq.1**, in °C.day^{-1}), and d) summed-up contribution of all oceanic processes ($B + C$ in **Eq.1**, in °C.day^{-1}). All terms are longitudinally averaged within the 1°-wide coastal band from 7°S to 4°S.

In conclusion, this analysis clearly shows a competition between two main terms: air-sea heat flux and vertical diffusion at the base of the mixed-layer, but the latter controls the seasonal variations of the MLT along the Congolese coast.

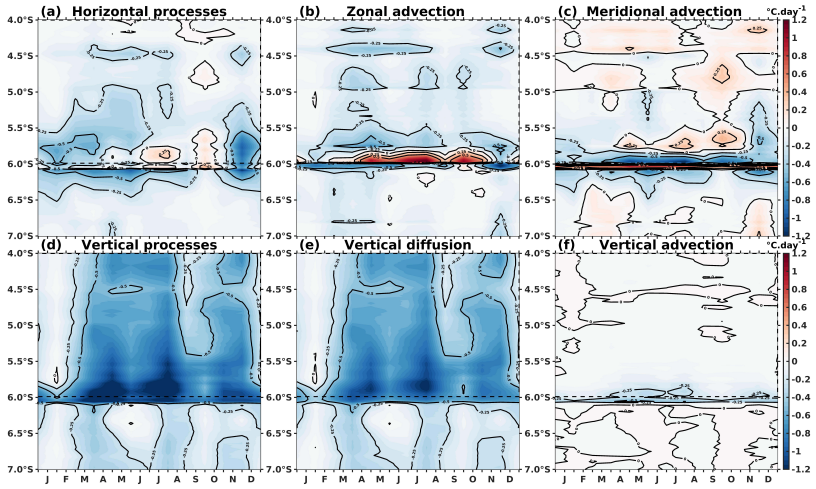

Figure 7. Model seasonal coastal mixed-layer heat budget (°C.day^{-1}) for the year 2016: a) summed-up contribution of horizontal oceanic processes (*B* in **Eq.1**), b) zonal advection, c) meridional advection, d) sum of sum of all vertical oceanic processes (*D* in **Eq.1**), e) vertical diffusion, and f) vertical advection. All terms are longitudinally averaged within the 1°-wide coastal band from 7°S to 4°S.

3.2.2 Seasonal variations of subsurface processes

We have shown that vertical diffusion is the main process that can explain the mixed-layer cooling in March-July season. We now assess the possible link between the mixed-layer cooling and the subsurface dynamics in the Congolese upwelling system (**Figure 8**). This is also an indication of the sensitivity of the MLD criterion.

Figure 8a shows similar characteristics to **Figure 4a-b** with a dominant semi-annual seasonal cycle, although the year 2016 is slightly warm compared to the 2007-2016 climatology. In **Figure 8b**, the temperature tendency term over the vertical shows a cooling over a long period between March and July from the surface to at least 50 m depth. We observe a further cooling in November-December below 5-10 m. On the other hand, we observe a warming between 0-50 m in January-February, a stronger warming around September, which persists from surface to the bottom. Here, we see that the role of vertical oceanic processes involved in the surface cooling differs from that in the subsurface. Vertical diffusion (**Figure 8c**) strongly cools the mixed-layer, which largely offsets the strong warming effect of the heat fluxes. Below the mixed-layer, it generally warms the subsurface but sometimes cools it, at certain depths and seasons. Vertical advection (**Figure 8d**) warms the water between 15-50 m and 30-50 m, in January-February and September, respectively. Otherwise, vertical advection predominantly cools the water column, and this cooling is most pronounced below the mixed-layer in the 5-15m interval approximately from March to July, and around December. From this subsurface analysis, it can be concluded that vertical mixing cooling is mostly confined to the mixed-layer throughout the seasonal cycle.

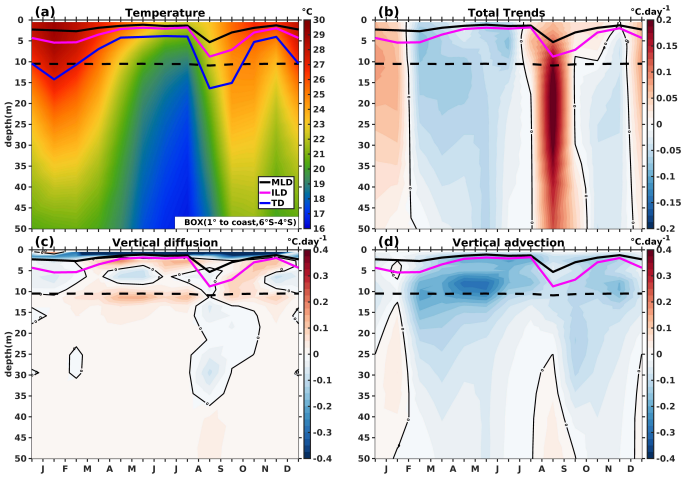

Figure 8. Subsurface (0-50m) model coastal seasonal heat budget for the year 2016, averaged within the 6°S-4°S 1°-wide coastal box (red contour in **Fig.1**): a) temperature (°C), b) temperature tendency (°C.day^{-1}), c) vertical diffusion (°C.day^{-1}), and d) vertical advection (°C.day^{-1}). Black, magenta, and blue lines denote the MLD, ILD, and TD, respectively. The dashed black line represents the MLD calculated online according to the density criterion with a threshold of 0.01 kg/m^{-3} and a reference depth of 10 m.

Note that the effect of vertical mixing on the MLT (within term D of **Eq.1**) depends on both the parameterized vertical diffusion coefficient noted k_z and the vertical temperature gradient at the MLD. The former is not directly calculated as a function of the Richardson number Ri with the GLS turbulent closure scheme used in the model. In the following, we start our analysis with the seasonal cycle of stratification and vertical shear of horizontal currents along the vertical in the CUS, which can modulate variations in surface-subsurface exchanges on a seasonal scale and thus affect the vertical mixing. On the one hand, the seasonal cycle of stratification is quantified by the Brunt Vaïsala N^2 frequency (**Figure 9a**), which presents two peaks in April-May and then in November-December, more pronounced at the surface around 5m. The stratification is mostly controlled by the salinity stratification N_S^2 rather than the temperature stratification N_T^2 (not shown), due to the high freshwater contribution from precipitation and runoffs (mainly dominated by the Congo River). In May, the rise of the thermocline brings cold and salty (and therefore dense) waters from the bottom to the near-surface, which explains the increase in the vertical gradient in temperature, salinity, and density, and therefore of N^2. On the other hand, the total shear Sh^2 (**Figure 9b**) also undergoes two peaks in March-April and October-November, in agreement with the surface wind regime at the coast (**Figure 9c**). Its effect is also more intense at the surface, at about 5 m. When decomposed into zonal shear Sh_u^2 and meridional shear Sh_v^2 (not shown), we find that both components seem to contribute to the seasonal changes in total shear, but its maximum in October-November can be mainly attributed to the meridional shear, in phase with the peaks of the meridional wind stress (**Figure 9c**), which are stronger than the peaks of the zonal wind stress. The Richardson number, Ri, defined as the ratio of buoyant suppression of turbulence to the shear generation of turbulence N^2/Sh^2, is used to quantify the dynamic stability. The minima of Ri (red contour in **Figure 9f**), with deep extension, agree well with the maxima of local wind stress (**Figure 9c**) in March and October. During the rest of the year, stratification largely dominates over shear at

depth, and to a lesser extent near the surface during the cooling period, thus limiting mixing, which suggests that the shear of the wind-driven flow alone cannot explain the increased vertical diffusion in the heat budget during austral winter. In addition, k_z (**Figure 9f**) and Ri (contours in **Figure 9f**) show a close relationship, with opposite variations. However, the seasonal cycle of the vertical temperature gradient (**Figure 9e**) is closely related to variations in the thermocline depth (blue line superimposed on **Figures 9d and 9e**), which are largely controlled by vertical currents (**Figure 9d**). Indeed, vertical mixing-driven seasonal cooling is strong when the thermocline is shallow (and wind stress is weak) and weak when the thermocline is deep (and wind stress is strong).

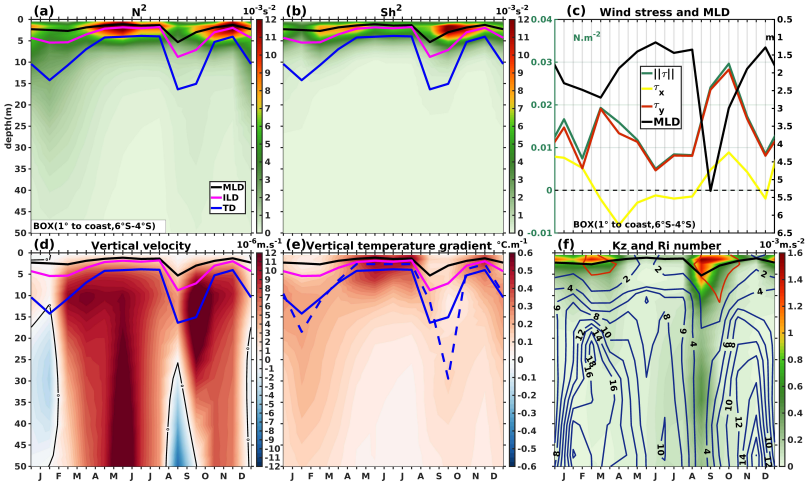

Figure 9. Model monthly climatology of vertical profiles (0-50 m), wind stress, and MLD for the year 2016 averaged within the 6°S-4°S 1°-wide coastal box (red contour in **Fig.1**): a) Brunt Vaïsäla frequency (N^2, in $10^{-3}s^2$), b) total square vertical shear (Sh^2, in $10^{-3}s^2$), c) wind stress ($N.m^{-2}$) magnitude (green) with zonal (blue) and meridional (red) contributions, and MLD (black, in m), d) vertical velocity (in $10^{-6}m.s^{-1}$), e) vertical temperature gradient (in $°C.m^{-1}$), and f) vertical diffusion coefficient $\boldsymbol{k_z}$ (colors, in $m.s^{-2}$) and Richardson number (Ri, contours, unitless). The red contours in panel f highlight $Ri = 1$. In panels a, b, d, and e, the black, magenta, and blue lines denote the MLD, ILD, and TD respectively. The dashed blue line in panel e shows the TD obtained from spatially averaged monthly profiles.

The above results suggest the importance of remote forcing. Indeed, the k_z and the local wind stress are in phase along the cycle, with the weak k_z values occurring during the seasonal cooling. In addition, the analysis of the seasonal cycle of the modeled SLA (**Figure 3d-e**) and thermocline depth (**Figure 3c-f**) clearly shows the semi-annual cycle of gravity waves propagating eastward along the equator and then southward along the African coast as CTWs, with strong upwelling (negative SLA and shallower TD) during the austral winter surface cooling (**Figures 6b and 8b**), between two downwelling phases (positive SLA and deeper TD). The upwelling associated with the CTWs is concomitant with the upward vertical velocities from April to August (**Figure 9d**), the rise of the thermocline and the strengthening of the vertical temperature gradient at the base of the mixed layer (**Figure 9e**), and the resulting mixed-layer cooling by vertical mixing.

4 Discussion

We investigated the seasonal changes of the MLT in the CUS, in a 6°S-4°S 1°-wide coastal box just north of the Congo estuary, and in particular the austral winter cooling leading to SSTs as cold as ~22°C, through the mixed-layer heat budget of a high-resolution oceanic model. The heat budget analysis reveals a competition between two main processes, as other tendency terms are relatively negligible (**Figures 6 and 7**). These processes are the surface forcing dominated by incoming solar flux (**Figure 6a**), which is counterbalanced by vertical mixing at the base of the mixed-layer (**Figure 7e**). The second one is the main driver of the austral winter cooling.

Air-sea heat flux is dominated by incoming solar flux and therefore tends to warm the mixed-layer all year long in our region. This warming is stronger around the Congo River mouth probably due to the thin mixed-layer associated with by the strong salinity stratification in the river plume (**Figure 9a-b**). Previously, Scannell and McPhaden (2018), using in situ measurements at the PIRATA mooring about 500 km off the mouth of the Congo River, found that the latent heat flux drives the cooling of the mixed-layer in austral winter. Herbert and Bourlès (2018), using an oceanic model, found the same result in a large coastal box (5°E-14°E;7°S-0°N) including both the mooring and our own box in the South-East corner. These results differ from ours but there is no contradiction. Indeed, recently, Körner et al. (2023) also did, from combined satellite and *in situ* data, a comparative mixed-layer heat budget between an offshore and a coastal box located in the Angola region south of ours (15°S-8°S). They found that the solar flux warming is stronger while the latent heat flux cooling is weaker in the coastal box relatively to the offshore box, respectively due to a stronger cloud cover away from the coast, and weaker wind near the coast. ASCAT satellite winds that are used to force our model were specifically selected to include this wind drop-off at the coast, due to increased friction with land, that can notably affect coastal upwelling through Ekman pumping in the Benguela region (Fennel et al., 2012). These cross-shore variations result, in the Angola upwelling system, in net air-sea heat fluxes that can cool the ocean for a few months offshore but warm it all year long at the coast, especially when combined with the salinity stratification effect, like in our region. This is also in agreement with the study of Lübbecke et al. (2019) in the Angola region, which explain the warm event in early 2016 by the combined action of reduced latent heat flux due to weakened wind and the freshwater input due to local precipitation and river discharge (dominated by the Congo River). Note however that the net downward air-sea heat flux could be overestimated in the model, as suggested by the 1°C warm offshore SST bias in the model compared to satellite data (**Figure 1a-b**), although this bias is reduced at the coast (**Figure 2a-b**).

However, cooling by vertical mixing exceeds warming by air-sea fluxes between March and July, which then leads to mixed-layer cooling along the Congolese coast (**Figure 6**). To understand the vertical mixing-induced cooling, we have examined the influence of local and remote forcing at seasonal scale. Comparison of seasonal variations of the vertical shear of horizontal currents, controlled by wind stress, and the mostly salinity-driven stratification shows that the former does not dominate over the latter during the cooling season (**Figure 9**). Indeed, wind stress peaks in March and October when vertical temperature diffusion is weak and, conversely, vertical temperature diffusion becomes strong from May to August when wind stress is weak (**Figures 7e and 9a-b-c**) north of 6°S. The salinity-driven stratification due to strong freshwater inputs from precipitation and Congo River influence the vertical mixing through the

barrier layer. The latter is particularly thick in March and October (**Figure 8**) which, despite strong wind-driven mixing, inhibits the heat exchanges between the surface and subsurface (Materia et al., 2012; Scannell and McPhaden, 2018; Lübbecke et al., 2019; Dossa et al., 2019; Houndegnonto et al., 2021). The seasonal maxima in vertical temperature diffusion, in May-August and November-December (**Figure 7e**), match those of the vertical temperature gradient at the base of the MLD, when the thermocline depth is shallower (**Figure 9e**). Along the equator and the southern African coast, the seasonal variations of sea level and thermocline anomalies are often associated with the eastward and southward propagation of CTW respectively (Herbert and Bourlès, 2018; Lübbecke et al., 2019). These waves have a semi-annual cycle, characterized by downwelling CTWs (reflected by positive SLA and deep thermocline) passing by our region around February, followed by upwelling CTWs (negative SLA and shallow thermocline) from April to August, then downwelling CTWs again in October and weaker downwelling CTWs in December (**Figure 3**). The CTW signature can be followed further south along the Angola coast (Awo et al., 2022). During austral winter, the upwelling CTWs lead to a shallow thermocline inducing a strong vertical temperature gradient in the upper 10 m which, combined with the relatively weak wind-induced mixing, results in the surface cooling and seasonal SST minimum in the CUS. The influence of EKW on SST seasonal changes have been already found further south in the Angola and Benguela upwelling systems (Ostrowski et al., 2009; Bachèlery et al., 2016, 2020). Also north of the CUS, between 3°S-0°N, Herbert and Bourlès (2018) have shown that surface cooling events in 2005 and 2006 were influenced by subsurface oceanic conditions the arrival of upwelling EKW.

From our subsurface analysis, we have identified two main vertical oceanic processes that can cool the upper ocean: vertical diffusion (**Figure 8c**) and vertical advection (**Figure 8d**). The former has a strong cooling effect limited to the upper 3 m all year long, maximum from April to August, but often a weak warming effect below and particularly at 10 m depth. The latter has mostly a cooling effect in the upper 50 m, particularly strong around 10 m from April to August, which is associated with the rise of the thermocline by upwelling CTWs discussed above (strong vertical temperature gradient and upward current in **Figures 9d** and **9e**). The relative contribution of these two processes to the mixed-layer temperature variations is highly dependent on the definition of the MLD, and particularly the chosen reference depth, which is still the subject of a debate in the GG. In this region, earlier mixed-layer heat budget studies based on model or observation often used a density criteria relative to a reference depth of 10 m (Materia et al., 2012; White and Toumi, 2014; Lübbecke et al., 2019; Kanga et al., 2021; Alory et al., 2021), as globally recommended by de Boyer Montégut et al. (2004) to avoid diurnal variations when MLD is estimated from Argo profiles. However, in our highly stratified Congo River plume region, the MLD computed online in the model with this reference depth and a density criterion of 0.01 kg/m^{-3} is almost constant and very close to 10 m (**Figure 8**). Vertical advection would be considered the dominant cooling term for the mixed layer in this case. But the thermocline is often shallower than 10 m, which is inconsistent, and the vertical shear from the wind-driven current is concentrated in a thinner layer (**Figure 9b**). This strongly suggests that the MLD should be computed differently. Therefore, we defined the MLD with a reference depth at the surface (actually 0.5 m that is the first depth level in the model), like other recent studies around the Congo plume region (Scannell & McPhaden, 2018; Körner et al., 2023), which puts the emphasis on the dominant role of vertical diffusion on the cooling in the mixed layer.

5 Conclusions

A high-resolution regional ocean model is used to investigate the seasonal changes of mixed-layer temperature in the Congolese upwelling system, north of the Congo River. The modeled heat budget within the mixed-layer analysis allows to identify the main processes driving these seasonal variations.

The model compares well with available observations in terms of spatial and seasonal variations of oceanic variables and remotely-forced coastal trapped waves along the coast.

The mixed-layer heat budget analysis reveals a competition between warming by heat fluxes, dominated all year long by the solar flux, and cooling by the vertical mixing at the base of the mixed layer, since other tendency terms are weak throughout the seasonal cycle. The seasonal cooling is induced by vertical mixing, though not controlled by the local wind. A subsurface analysis shows that remotely-forced coastally trapped waves rise the thermocline from April to August, which strengthens the vertical temperature gradient at the mixed layer base and leads to the mixing-induced seasonal cooling in the Congolese upwelling system. These main driving processes, deduced from our model, are similar to those deduced from a recent observation-based study for the Angola upwelling system further south, on the other side of the Congo River mouth (Körner et al., 2023).

However, in the Angola upwelling system, Zeng et al. (2021) have suggested that internal tides can induce the strong mixing in shallow area then cool the mixed layer near the coast. By using microstructure measurements of shear to estimate turbulent heat fluxes, Körner et al. (2023) have indeed found that the cooling due to turbulent mixing at the base of the mixed layer is stronger at the coast in the shallow area than offshore. Our model can reproduce the seasonal cooling without tides, but a twin experiment including tidal forcing could be conducted to evaluate the contribution of internal tides in the CUS. Recently, Alory et al. (2021) and Topé et al. (2023) used paired simulations with and without rivers to quantify the role of the Niger River discharge along the northern coast of the Gulf of Guinea. Their results show that the river runoff induces warming by reducing the vertical mixing and the onshore meridional advection. There are contrasting results on the Congo River effect suggesting either SST warming (Materia et al., 2012) or cooling (White and Toumi, 2014) and we plan to evaluate this effect on the mixed-layer heat budget in our model, with sensitivity experiments now available. We could also modify the equatorial wind forcing in our model to suppress EKW and quantify their effects along the Congolese coast. Finally, a reference coupled physical-biogeochemical simulation based on our model configuration is in preparation, which would help to assess the respective biological contribution of upwelling and Congo River nutrient input in our region.

Acknowledgments

This work is part of Roy Dorgeless Ngakala's Ph.D. thesis funded by the German Academic Exchange Service (DAAD) under the In-Country/In-Region Scholarship Program for Sub-Saharan Africa. This study has benefited from product sets freely available, we thank these diverse platforms and in particular SNO-SSS and PIRATA. We also thank the TRIATLAS project funded by the European Union's Horizon 2020 research and innovation program under

grant agreement 817578 and the TOSCA SMOS and SWOT-GG projects funded by the CNES for their various supports. Computing resources are provided by DARI under grant GEN7298.

Data Availability Statement

All products used here are publicly available, and some require free registration. The MUR SST product created by the JPL MUR MEaSURES program as part of the GHRSST (Group for High-Resolution Sea Surface Temperature) project is obtained from https://podaac.jpl.nasa.gov/dataset/MUR-JPL-L4-GLOB-v4.1. The SMAP SSS product created by JPL (Jet Propulsion Laboratory) is available at https://podaac.jpl.nasa.gov/dataset/SMAP_JPL_L2B_SSS_CAP_V5. The CMEMS (COPERNICUS MARINE ENVIRONMENT MONITORING SERVICE) SSHproduct produced by SSALTO/DUAC is available at http://marine.copernicus.eu/. TSG SSS product managed by SNO-SSS/SEDOO is available at http://sss.sedoo.fr/. PIRATA surface and subsurface data are from the ftp site ftp://ftp.ifremer.fr/ifremer/ird/pirata/pirata-data/. The WOA data are from NOAA/NCEI via https://www.nodc.noaa.gov/OC5/woa18/. Model outputs are available from the authors, especially GA, ID, GM and JJ.

References

Alory, G., Delcroix, T., Téchiné, P., Diverrès, D., Varillon, D., Cravatte, S., Gouriou, Y., Grelet, J., Jacquin, S., Kestenare, E., Maes, C., Morrow, R., Perrier, J., Reverdin, G., and Roubaud, F.: The French contribution to the voluntary observing ships network of sea surface salinity, Deep Sea Res. Part I Oceanogr. Res. Pap., 105, 1–18, https://doi.org/10.1016/j.dsr.2015.08.005, 2015.

Alory, G., Da-Allada, C. Y., Djakouré, S., Dadou, I., Jouanno, J., and Loemba, D. P.: Coastal Upwelling Limitation by Onshore Geostrophic Flow in the Gulf of Guinea Around the Niger River Plume, Front. Mar. Sci., 7, 1–17, https://doi.org/10.3389/fmars.2020.607216, 2021.

Awo, F. M., Rouault, M., Ostrowski, M., Tomety, F. S., Da-Allada, C. Y., and Jouanno, J.: Seasonal Cycle of Sea Surface Salinity in the Angola Upwelling System, J. Geophys. Res. Ocean., 127, 1–13, https://doi.org/10.1029/2022JC018518, 2022.

Bachèlery, M., Illig, S., and Dadou, I.: Interannual variability in the S outh-E ast A tlantic O cean, focusing on the B enguela U pwelling S ystem: Remote versus local forcing, J. Geophys. Res. Ocean., 121, 284–310, 2016.

Bachèlery, M. Lou, Illig, S., and Rouault, M.: Interannual Coastal Trapped Waves in the Angola-Benguela Upwelling System and Benguela Niño and Niña events, J. Mar. Syst., 203, 0–46, https://doi.org/10.1016/j.jmarsys.2019.103262, 2020.

Bentamy, A. and Fillon, D. C.: Gridded surface wind fields from Metop/ASCAT measurements, Int. J. Remote Sens., 33, 1729–1754, https://doi.org/10.1080/01431161.2011.600348, 2012.

Berrit, G. R.: Les eaux froides cotieres du Gabon a L'Angola sont-elles dues a un upwelling d'Ekman, Cah. ORSTOM Séries Océanographie, 14, 273–278, 1976.

Bordbar, M. H., Mohrholz, V., and Schmidt, M.: The Relation of Wind-Driven Coastal and

707 Offshore Upwelling in the Benguela Upwelling System, J. Phys. Oceanogr., 51, 3117–3133,
708 https://doi.org/10.1175/JPO-D-20-0297.1, 2021.

709 Bourlès, B., Araujo, M., McPhaden, M. J., Brandt, P., Foltz, G. R., Lumpkin, R., Giordani, H.,
710 Hernandez, F., Lefèvre, N., Nobre, P., Campos, E., Saravanan, R., Trotte-Duhà, J., Dengler, M.,
711 Hahn, J., Hummels, R., Lübbecke, J. F., Rouault, M., Cotrim, L., Sutton, A., Jochum, M., and
712 Perez, R. C.: PIRATA: A Sustained Observing System for Tropical Atlantic Climate Research
713 and Forecasting, Earth Sp. Sci., 6, 577–616, https://doi.org/10.1029/2018EA000428, 2019.

714 de Boyer Montégut, C., Madec, G., Fischer, A. S., Lazar, A., and Iudicone, D.: Mixed layer
715 depth over the global ocean: An examination of profile data and a profile-based climatology, J.
716 Geophys. Res. Ocean., 109, 1–20, https://doi.org/10.1029/2004JC002378, 2004.

717 Brandt, P., Alory, G., Awo, F. M., Dengler, M., Djakouré, S., Imbol Koungue, R. A., Jouanno,
718 J., Körner, M., Roch, M., and Rouault, M.: Physical processes and biological productivity in the
719 upwelling regions of the tropical Atlantic, Ocean Sci., 19, 581–601, https://doi.org/10.5194/os-
720 19-581-2023, 2023.

721 Camara, I., Kolodziejczyk, N., Mignot, J., Lazar, A., and Gaye, A. T.: On the seasonal variations
722 of salinity of the tropical Atlantic mixed layer, J. Geophys. Res. Ocean., 120, 4441–4462,
723 https://doi.org/https://doi.org/10.1002/2015JC010865, 2015.

724 Carr, M. E. and Kearns, E. J.: Production regimes in four Eastern Boundary Current systems,
725 Deep. Res. Part II Top. Stud. Oceanogr., 50, 3199–3221,
726 https://doi.org/10.1016/j.dsr2.2003.07.015, 2003.

727 Chavez, F. P. and Messié, M.: A comparison of Eastern Boundary Upwelling Ecosystems, Prog.
728 Oceanogr., 83, 80–96, https://doi.org/10.1016/j.pocean.2009.07.032, 2009.

729 Chin, T. M., Vazquez-Cuervo, J., and Armstrong, E. M.: A multi-scale high-resolution analysis
730 of global sea surface temperature, Remote Sens. Environ., 200, 154–169,
731 https://doi.org/10.1016/j.rse.2017.07.029, 2017.

732 Da-Allada, C. Y., du Penhoat, Y., Jouanno, J., Alory, G., and Hounkonnou, N. M.: Modeled
733 mixed-layer salinity balance in the Gulf of Guinea: seasonal and interannual variability, Ocean
734 Dyn., 64, 1783–1802, https://doi.org/10.1007/s10236-014-0775-9, 2014.

735 Decharme, B., Delire, C., Minvielle, M., Colin, J., Vergnes, J., Alias, A., Saint-Martin, D.,
736 Séférian, R., Sénési, S., and Voldoire, A.: Recent changes in the ISBA-CTRIP land surface
737 system for use in the CNRM-CM6 climate model and in global off-line hydrological
738 applications, J. Adv. Model. Earth Syst., 11, 1207–1252, 2019.

739 Denamiel, C., Budgell, W. P., and Toumi, R.: The congo river plume: Impact of the forcing on
740 the far-field and near-field dynamics, J. Geophys. Res. Ocean., 118, 964–989,
741 https://doi.org/10.1002/jgrc.20062, 2013.

742 Deppenmeier, A.-L., Haarsma, R. J., van Heerwaarden, C., and Hazeleger, W.: The Southeastern
743 Tropical Atlantic SST Bias Investigated with a Coupled Atmosphere–Ocean Single-Column

744 Model at a PIRATA Mooring Site, J. Clim., 33, 6255–6271, 2020.

745 Dieng, H. B., Dadou, I., Léger, F., Morel, Y., Jouanno, J., Lyard, F., and Allain, D.: Sea level
746 anomalies using altimetry, model and tide gauges along the African coasts in the Eastern
747 Tropical Atlantic Ocean: Inter-comparison and temporal variability, Adv. Sp. Res., 68, 534–552,
748 https://doi.org/10.1016/j.asr.2019.10.019, 2021.

749 Dossa, A. N., Da-Allada, C. Y., Herbert, G., and Bourlès, B.: Seasonal cycle of the salinity
750 barrier layer revealed in the northeastern Gulf of Guinea, African J. Mar. Sci., 41, 163–175,
751 https://doi.org/10.2989/1814232X.2019.1616612, 2019.

752 Ducet, N., Le Traon, P. Y., and Reverdin, G.: Global high-resolution mapping of ocean
753 circulation from TOPEX/Poseidon and ERS-1 and -2, J. Geophys. Res. Ocean., 105, 19477–
754 19498, https://doi.org/10.1029/2000JC900063, 2000.

755 Fennel, W., Junker, T., Schmidt, M., and Mohrholz, V.: Response of the Benguela upwelling
756 systems to spatial variations in the wind stress, Cont. Shelf Res., 45, 65–77,
757 https://doi.org/10.1016/j.csr.2012.06.004, 2012.

758 Foltz, G. R., Grodsky, S. A., Carton, J. A., and McPhaden, M. J.: Seasonal mixed layer heat
759 budget of the tropical Atlantic Ocean, J. Geophys. Res. Ocean., 108,
760 https://doi.org/https://doi.org/10.1029/2002JC001584, 2003.

761 Fore, A. G., Yueh, S. H., Tang, W., Stiles, B. W., and Hayashi, A. K.: Combined Active/Passive
762 Retrievals of Ocean Vector Wind and Sea Surface Salinity With SMAP, IEEE Trans. Geosci.
763 Remote Sens., 54, 7396–7404, https://doi.org/10.1109/TGRS.2016.2601486, 2016.

764 Gaillard, F., Diverres, D., Jacquin, S., Gouriou, Y., Grelet, J., Le Menn, M., Tassel, J., and
765 Reverdin, G.: Sea surface temperature and salinity from French research vessels, 2001–2013,
766 Sci. Data, 2, 150054, https://doi.org/10.1038/sdata.2015.54, 2015.

767 Garcia, H. E., Boyer, T. P., Baranova, O. K., Locarnini, R. A., Mishonov, A. V, Grodsky, A. ea,
768 Paver, C. R., Weathers, K. W., Smolyar, I. V, and Reagan, J. R.: World ocean atlas 2018:
769 Product documentation, A. Mishonov, Tech. Ed., 1, 1–20, 2019.

770 Gutknecht, E., Dadou, I., Le Vu, B., Cambon, G., Sudre, J., Garçon, V., MacHu, E., Rixen, T.,
771 Kock, A., Flohr, A., Paulmier, A., and Lavik, G.: Coupled physical/biogeochemical modeling
772 including O2-dependent processes in the Eastern Boundary Upwelling Systems: Application in
773 the Benguela, Biogeosciences, 10, 3559–3591, https://doi.org/10.5194/bg-10-3559-2013, 2013.

774 Herbert, G. and Bourlès, B.: Impact of intraseasonal wind bursts on sea surface temperature
775 variability in the far eastern tropical Atlantic Ocean during boreal spring 2005 and 2006: Focus
776 on the mid-May 2005 event, Ocean Sci., 14, 849–869, https://doi.org/10.5194/os-14-849-2018,
777 2018.

778 Hopkins, J., Lucas, M., Dufau, C., Sutton, M., Stum, J., Lauret, O., and Channelliere, C.:
779 Detection and variability of the Congo River plume from satellite derived sea surface
780 temperature, salinity, ocean colour and sea level, Remote Sens. Environ., 139, 365–385,

781 https://doi.org/10.1016/j.rse.2013.08.015, 2013.

782 Houndegnonto, O. J., Kolodziejczyk, N., Maes, C., Bourlès, B., Da-Allada, C. Y., and Reul, N.:
783 Seasonal Variability of Freshwater Plumes in the Eastern Gulf of Guinea as Inferred From
784 Satellite Measurements, J. Geophys. Res. Ocean., 126, 1–27,
785 https://doi.org/10.1029/2020JC017041, 2021.

786 Illig, S.: Interannual long equatorial waves in the tropical Atlantic from a high-resolution ocean
787 general circulation model experiment in 1981–2000, J. Geophys. Res., 109, C02022,
788 https://doi.org/10.1029/2003JC001771, 2004.

789 Illig, S., Bachèlery, M. Lou, and Lübbecke, J. F.: Why Do Benguela Niños Lead Atlantic
790 Niños?, J. Geophys. Res. Ocean., 125, https://doi.org/10.1029/2019JC016003, 2020.

791 Jean-Michel, L., Eric, G., Romain, B. B., Gilles, G., Angélique, M., Marie, D., Clément, B.,
792 Mathieu, H., Olivier, L. G., Charly, R., Tony, C., Charles-Emmanuel, T., Florent, G., Giovanni,
793 R., Mounir, B., Yann, D., and Pierre-Yves, L. T.: The Copernicus Global 1/12° Oceanic and Sea
794 Ice GLORYS12 Reanalysis, Front. Earth Sci., 9, 1–27,
795 https://doi.org/10.3389/feart.2021.698876, 2021.

796 Jouanno, J., Marin, F., Du Penhoat, Y., Sheinbaum, J., and Molines, J. M.: Seasonal heat balance
797 in the upper 100 m of the equatorial Atlantic Ocean, J. Geophys. Res. Ocean., 116, 1–19,
798 https://doi.org/10.1029/2010JC006912, 2011.

799 Kanga, D. K., Kouassi, M. A., Trokourey, A., Toualy, E., N'Guessan, B. K., Brehmer, P., and
800 Ostrowski, M.: Spatial and seasonal variability of mixed layer depth in the tropical Atlantic at 10
801 W using 40 years of observation data, Eur. J. Sci. Res., 2021.

802 Kobayashi, S., Ota, Y., Harada, Y., Ebita, A., Moriya, M., Onoda, H., Onogi, K., Kamahori, H.,
803 Kobayashi, C., Endo, H., Miyaoka, K., and Kiyotoshi, T.: The JRA-55 reanalysis: General
804 specifications and basic characteristics, J. Meteorol. Soc. Japan, 93, 5–48,
805 https://doi.org/10.2151/jmsj.2015-001, 2015.

806 Körner, M., Brandt, P., and Dengler, M.: Seasonal cycle of sea surface temperature in the
807 tropical Angolan Upwelling System, Ocean Sci., 19, 121–139, https://doi.org/10.5194/os-19-
808 121-2023, 2023.

809 Kurian, J., Li, P., Chang, P., Patricola, C. M., and Small, J.: Impact of the Benguela coastal low-
810 level jet on the southeast tropical Atlantic SST bias in a regional ocean model, Clim. Dyn., 56,
811 2773–2800, https://doi.org/10.1007/s00382-020-05616-5, 2021.

812 Laraque, A., N'kaya, G. D. M., Orange, D., Tshimanga, R., Tshitenge, J. M., Mahé, G.,
813 Nguimalet, C. R., Trigg, M. A., Yepez, S., and Gulemvuga, G.: Recent budget of
814 hydroclimatology and hydrosedimentology of the congo river in central Africa, Water
815 (Switzerland), 12, https://doi.org/10.3390/w12092613, 2020.

816 Lübbecke, J. F., Brandt, P., Dengler, M., Kopte, R., Lüdke, J., Richter, I., Sena Martins, M., and
817 Tchipalanga, P. C. M.: Causes and evolution of the southeastern tropical Atlantic warm event in

early 2016, Clim. Dyn., 53, 261–274, https://doi.org/10.1007/s00382-018-4582-8, 2019.

Madec, G., Bourdallé-Badie, R., Bouttier, P.-A., Bricaud, C., Bruciaferri, D., Calvert, D., Chanut, J., Clementi, E., Coward, A., and Delrosso, D.: NEMO ocean engine, 2017.

Martins, M. S. and Stammer, D.: Interannual Variability of the Congo River Plume-Induced Sea Surface Salinity, Remote Sens., 14, https://doi.org/10.3390/rs14041013, 2022.

Materia, S., Gualdi, S., Navarra, A., and Terray, L.: The effect of Congo River freshwater discharge on Eastern Equatorial Atlantic climate variability, Clim. Dyn., 39, 2109–2125, https://doi.org/10.1007/s00382-012-1514-x, 2012.

Ngakala, R. D., Alory, G., Da-Allada, C. Y., Kom, O. E., Jouanno, J., Rath, W., and Baloïtcha, E.: Joint observation-model mixed-layer heat and salt budgets in the eastern tropical Atlantic, Ocean Sci., 19, 535–558, https://doi.org/10.5194/os-19-535-2023, 2023.

Ostrowski, M., Da Silva, J. C. B., and Bazik-Sangolay, B.: The response of sound scatterers to El Ninõ- and La Niña-like oceanographic regimes in the southeastern Atlantic, ICES J. Mar. Sci., 66, 1063–1072, https://doi.org/10.1093/icesjms/fsp102, 2009.

Peter, A. C., Le Hénaff, M., du Penhoat, Y., Menkes, C. E., Marin, F., Vialard, J., Caniaux, G., and Lazar, A.: A model study of the seasonal mixed layer heat budget in the equatorial Atlantic, J. Geophys. Res. Ocean., 111, 1–16, https://doi.org/10.1029/2005JC003157, 2006.

Pham, H. T. and Sarkar, S.: Ageostrophic Secondary Circulation at a Submesoscale Front and the Formation of Gravity Currents, J. Phys. Oceanogr., 48, 2507–2529, https://doi.org/10.1175/JPO-D-17-0271.1, 2018.

Piton, B.: Les courants sur le plateau continental devant Pointe-Noire (Congo), Doc. Sci. ORSTOM, Brest, 37, 1988.

Richter, I.: Climate model biases in the eastern tropical oceans: causes, impacts and ways forward, WIREs Clim. Chang., 6, 345–358, https://doi.org/10.1002/wcc.338, 2015.

Rouault, M., Servain, J., Reason, C. J. C., Bourlès, B., Rouault, M. J., and Fauchereau, N.: Extension of PIRATA in the tropical South-East Atlantic: an initial one-year experiment, African J. Mar. Sci., 31, 63–71, 2009.

Scannell, H. A. and McPhaden, M. J.: Seasonal Mixed Layer Temperature Balance in the Southeastern Tropical Atlantic, J. Geophys. Res. Ocean., 123, 5557–5570, https://doi.org/10.1029/2018JC014099, 2018.

Topé, G. D. A., Alory, G., Djakouré, S., Da-Allada, C. Y., Jouanno, J., and Morvan, G.: How does the Niger river warm coastal waters in the northern Gulf of Guinea?, Front. Mar. Sci., 10, 1–11, https://doi.org/10.3389/fmars.2023.1187202, 2023.

Le Traon, P. Y., Nadal, F., and Ducet, N.: An Improved Mapping Method of Multisatellite Altimeter Data, J. Atmos. Ocean. Technol., 15, 522–534, https://doi.org/10.1175/1520-

0426(1998)015<0522:AIMMOM>2.0.CO;2, 1998.

Umlauf, L. and Burchard, H.: A generic length-scale equation for geophysical turbulence models, J. Mar. Res., 61, 235–265, 2003.

Umlauf, L. and Burchard, H.: Second-order turbulence closure models for geophysical boundary layers. A review of recent work, Cont. Shelf Res., 25, 795–827, https://doi.org/10.1016/j.csr.2004.08.004, 2005.

Vic, C., Berger, H., Tréguier, A.-M., and Couvelard, X.: Dynamics of an Equatorial River Plume: Theory and Numerical Experiments Applied to the Congo Plume Case, J. Phys. Oceanogr., 44, 980–994, https://doi.org/10.1175/JPO-D-13-0132.1, 2014.

Voituriez, B. and Herbland, A.: Comparaison des systèmes productifs de l'Atlantique Tropical Est: dômes thermiques, upwellings côtiers et upwelling équatorial, Rapp. Procès-Verbaux des Réunions Cons. Int. pour l'Exploration la Mer, 180, 114–130, 1982.

Wacongne, S. and Piton, B.: The near-surface circulation in the northeastern corner of the South Atlantic ocean, Deep Sea Res. Part A. Oceanogr. Res. Pap., 39, 1273–1298, https://doi.org/10.1016/0198-0149(92)90069-6, 1992.

Wade, M., Caniaux, G., and Du Penhoat, Y.: Variability of the mixed layer heat budget in the eastern equatorial Atlantic during 2005-2007 as inferred using Argo floats, J. Geophys. Res. Ocean., 116, 1–17, https://doi.org/10.1029/2010JC006683, 2011.

White, R. H. and Toumi, R.: River flow and ocean temperatures: The Congo River, J. Geophys. Res. Ocean., 119, 2501–2517, https://doi.org/10.1002/2014JC009836, 2014.

Xu, Z., Chang, P., Richter, I., Kim, W., and Tang, G.: Diagnosing southeast tropical Atlantic SST and ocean circulation biases in the CMIP5 ensemble, Clim. Dyn., 43, 3123–3145, https://doi.org/10.1007/s00382-014-2247-9, 2014.

Zeng, Z., Brandt, P., Lamb, K. G., Greatbatch, R. J., Dengler, M., Claus, M., and Chen, X.: Three-Dimensional Numerical Simulations of Internal Tides in the Angolan Upwelling Region, J. Geophys. Res. Ocean., 126, 1–20, https://doi.org/10.1029/2020JC016460, 2021.